Point fields of last passage percolation and coalescing fractional Brownian motions

Konstantin Khanin, Liying Li,* and Zhanghan Yin
Department of Mathematics, University of Toronto, Toronto M5S 2E4, Canada

(Received 28 December 2021; accepted 1 June 2022; published 24 June 2022)

We consider large-scale point fields which naturally appear in the context of the Kardar-Parisi-Zhang (KPZ) phenomenon. Such point fields are geometrical objects formed by points of mass concentration, and by shocks separating the sources of these points. We introduce similarly defined point fields for processes of coalescing fractional Brownian motions (cfBMs). The case of the Hurst index 2/3 is of particular interest for us since, in this case, the power law of the density decay is the same as that in the KPZ phenomenon. In this paper, we present strong numerical evidence that statistical properties of points fields in these two different settings are very similar. We also discuss theoretical arguments in support of the conjecture that they are exactly the same in the large-time limit. This would indicate that two objects may, in fact, belong to the same universality class.

DOI: 10.1103/PhysRevE.105.064127

I. INTRODUCTION

The KPZ equation,

$$\partial_t h + \tfrac{1}{2}(\partial_x h)^2 = \nu \partial_{xx} h + F,$$
$$F = \text{ space-time white noise}, \tag{1}$$

describes the motion of growing surfaces that is subject to smoothing effects, slope-dependent growth speed, and space-time uncorrelated noise. In the seminal paper by Kardar, Parisi and Zhang [1], it was predicted that the fluctuations of the height function, $h(t,x)$, are of the order of $t^{1/3}$ and the spatial correlation occurs at the scale of $t^{2/3}$. The $1:2:3$ scaling, known as the KPZ scaling, also arises in many other models including random matrices, random growth models, interacting particle systems, optimal paths or directed polymers in random environments, and randomly forced Burgers equation or Hamilton-Jacobi equations [2–12].

Naturally, scaling exponents which describe the large-scale properties should not be affected by the roughness of the environment F; it is believed that a sufficient condition for the 2/3 transversal exponent is rapid space-time decorrelation of the random environment. In the following we will assume F to be smooth, which describes the large-scale properties with rapid space-time decorrelation.

Besides the height function, there is also a geometrical approach to understand the KPZ scaling through the geometrical properties of optimal paths or equivalent objects in these models. Such geometrical objects already arise when representing the solution to (1) via the Feynman-Kac formula after applying the Hopf-Cole transform $h(t,x) = -2\nu \ln \phi(t,x)$:

$$\phi(t,x) = \int e^{-\frac{1}{2\nu}\left[h(t,\gamma_0)+\int_0^t F(s,\gamma_s)\,ds\right]} W(dB), \tag{2}$$

where $\gamma_s = x + \sqrt{2\nu} B_{t-s}$, and $W(\cdot)$ is the standard Wiener measure.

The Gibbs measure on paths

$$P_0^{t,x}(d\gamma) = Z^{-1} e^{-\frac{1}{2\nu}\left[h(t,\gamma_0)+\int_0^t F(s,\gamma_s)\,ds\right]} W(dB)$$

is a *polymer measure* in the random environment given by F. Although $P_0^{t,x}$ is random, there exists a deterministic number $\chi \in [0,1]$, called the *transversal exponent*, such that the probability

$$P_0^{t,x}\big(\max_{0\leqslant s\leqslant t} |\gamma_s - \gamma_t| = O(t^{\chi})\big)$$

is close to 1 for a typical environment. The KPZ scaling corresponds to $\chi = 2/3$; for comparison, in the absence of randomness, i.e., $F = 0$, $P_0^{t,x}$ is equivalent to the Wiener measure and thus $\chi = 1/2$.

In the zero temperature limit $\nu \to 0$, the Gibbs measures will concentrate on geodesics that have a fixed endpoint $\gamma_t = x$ and minimize the action

$$h(0,\gamma_0) + \int_0^t [L(\dot{\gamma}_s) + F(s, x+\gamma_s)]\,ds, \quad L(p) = \frac{p^2}{2}. \tag{3}$$

The Lagrangian L can be other convex functions, and this optimization problem is the one that occurs in the Lax-Oleinik variational principle that gives the viscous solution to the inviscid Hamilton-Jacobi equation

$$\partial_t u + H(\partial_x u) = F(t,x),$$

where H is the Legendre dual of L. Compared to polymer measures, the geometry of geodesics is easier to describe because of fewer layers of randomness. The transversal exponent χ of the geodesics can be defined in a similar way: let $\gamma = \gamma^{t,x}$ be the geodesic; then in a typical environment

$$\max_{0\leqslant s\leqslant t} |\gamma_s - \gamma_t| = O(t^{\chi}).$$

In general, the models of finding optimal paths in random environments are called *first- or last-passage percolation* (FPP/LPP).

In most of the FPP/LPP models, geodesics cannot intersect except at the endpoints. In the context of Hamilton-Jacobi

*Corresponding author: liyingli@math.toronto.edu

 ©2022 American Physical Society

equations this means the following: let $\gamma^{1,2} : [0,t] \to \mathbb{R}$ be two geodesics of (3) (i.e., any perturbation of $\gamma^{1,2}$ will have higher action); then $\gamma^1(s) = \gamma^2(s)$ can only happen for $s = 0$ or t. This is due to the convexity of the Lagrangian L.

The nonintersecting property gives a monotone structure to the geodesics. In particular, the map $x \mapsto \gamma^x(0)$ is monotone (nondecreasing), where γ^x is the minimizing path of (3) with $\gamma(t) = x$. Although γ^x may not be unique, the monotone map is well defined since the discontinuity points are at most countable. Such points with more than one minimizers correspond to the formation of shocks.

We can obtain a consistent family of monotone maps $(\phi^{s,t})_{s<t}$ that satisfies $\phi^{r,s} \circ \phi^{s,t} = \phi^{r,t}$ for all $r < s < t$, if we look at infinite geodesics. More specifically, fix a large negative T and let $\gamma^{t,x}$ be the minimizing path of (3) that starts from time T and terminates at (t,x). The family of monotone maps is given by $\phi_T^{s,t}(x) = \gamma^{t,x}(s)$, $T < s < t$. By the principle of dynamic programming, these monotone maps are consistent:

$$\phi_T^{r,s} \circ \phi_T^{s,t} = \phi_T^{r,t}, \qquad T \leqslant s < t < r.$$

Sending $T \to -\infty$, we get rid of the dependence on T, and can think of obtaining these monotone maps from infinite geodesics. These monotone maps depend on the random environment, and since the environment is space-time stationary, so are the monotone maps; the temporal stationarity means that $\phi^{s+r,t+r}$ has the same statistics as $\phi^{s,t}$ for all r, and the spatial stationarity means that $x \mapsto \phi^{s,t}(x) - x$ is a stationary process. Since the transversal exponent for infinite geodesics should be the same as the finite ones, we can also see the KPZ scaling in terms of the monotone maps: $|\phi^{-t,0}(x) - x| = O(t^\chi)$, $\chi = 2/3$.

We are interested in understanding to what extent the monotonicity property and correlation structures determine the value of χ. More precisely, let $\phi^{s,t} : \mathbb{R} \to \mathbb{R}$, $s < t$, be a consistent, stationary flow of random monotone maps. Then, is it true that for some $\chi \geqslant 0$, $|\phi^{-t,0}(x) - x| = O(t^\chi)$? How does χ depend on the distribution of the monotone maps? Moreover, when χ exists, what is the scaling limit of the renormalized monotone maps $[\mathrm{R}_{L,\chi}\phi]^{s,t}(x) = L^{-\chi}\phi^{Ls,Lt}(L^\chi x)$, as $L \to \infty$? Is this limit uniquely determined by χ? We are particularly interested in the case $\chi = 2/3$, since this value of χ corresponds to the KPZ universality.

Another special case is $\chi = 1/2$. This case can be studied rigorously since the monotone maps $\phi^{s,t}$ are independent in time, and the scaling limit is given by the *coalescing Brownian motion* (cBM). However, from the geometrical perspective described above, neither the 2/3 nor 1/2 exponents should be special; it should be possible to obtain scaling limits for other values of χ by varying the temporal decay of correlation of the monotone maps.

Any scaling limit of the renormalization operator $R_{L,\chi}$ produces its fixed point. The fixed point for $\chi = 1/2$ is given by the flow of cBM, constructed as follows. Particles start from every position on the line at time s and perform independent Brownian motions until collision. When two particles collide, they merge into a new particle which continues to perform Brownian motion independent of other particles. For $s < t$, let $\phi^{s,t}(x)$ be the time-t position of the particle coming from

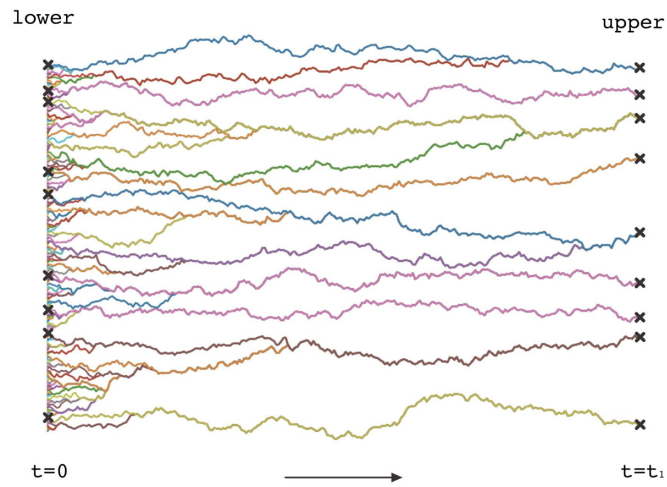

FIG. 1. Upper and lower point fields of a coalescing process.

location x at time s. The coalescing construction ensures that $(\phi^{s,t})_{s<t}$ is a family of monotone maps. Moreover, due to the memoryless effect (Markov property) of Brownian motions, if we follow the trajectory of one particle, $t \mapsto \phi^{s,t}(x)$, the trajectory is a Brownian path despite collisions taking place along the way, and it follows from the diffusive scaling of Brownian motions that $|\phi^{0,t}(x) - x| = O(t^{1/2})$ for the flow of cBM. By the invariance of Brownian motion it is not hard to see that it is a fixed point for $R_{L,1/2}$. Note the different time directions for these models: the flow of cBM is forward in time, while the infinite geodesics from Hamilton-Jacobi equations are backward in time.

The flow of cBM was first rigorously constructed by Arratia [13]. The most technical point was to show the "coalescence from infinity" property; that is, at every time $t > 0$, there are only countably many particles left at discrete positions. As a consequence, all the maps $\phi^{s,t}$ are piecewise constant functions that can be characterized by two discrete point fields

$$\cdots < a_{-1} < a_0 < a_1 < \cdots, \qquad \cdots < b_{-1} < b_0 < b_1 < \cdots$$

such that $\phi^{s,t}((a_n, a_{n+1})) = b_n$ for $n \in \mathbb{Z}$.

The "coalescence from infinity" property means that the random set of surviving particles at any positive time $t > 0$ constitutes a point field. We call this the *upper point field*. On the other hand, for each point in the upper point field, the set of starting positions that end up at that point is almost surely an interval. The endpoints of these intervals constitute the *lower point field* (Fig. 1).

It is known that for many FPP/LPP models the coalescence of infinite geodesics also takes place [14,15]; that is, denoting by γ^x the geodesic from x at time 0, for $x \neq y$, there is a (negative) time $T = T_{x,y}$ for which $|\gamma^x(T) - \gamma^y(T)| \ll 1$, and $|\gamma^x(t) - \gamma^y(t)|$ will converge exponentially fast for $t < T$. In fact, for the lattice model, $\gamma^x(t) = \gamma^y(t)$ for $t < T$. The time $T_{x,y}$ is called the coalescence time, and according to the KPZ scaling, for fixed x and S, the starting point y such that the coalescence time $|T_{x,y}| < S$ should be distance $O(S^{2/3})$ away from x. As a result, the fixed point of $R_{L,2/3}$ obtained from solvable KPZ models is also given by piecewise constant maps. In this paper we argue that the statistical properties of

this maps are determined by the monotonicity properties and the planar geometry.

In what follows, we numerically construct various candidates for the fixed point of $R_{L,2/3}$ from a new class of coalescing processes called the *coalescing fractional Brownian motion* (cfBM). We then compare the statistics of the upper/lower point fields to that obtained from solvable KPZ models, and observe that these models share strikingly similar statistics.

II. NUMERICAL EXPERIMENT

A. Coalescing fractional Brownian motion and exponential corner growth model

Intuitively, the construction of cfBM is similar to that of cBM: at the initial time $t = 0$, independent fractional Brownian particles of Hurst index $H \in (0, 1)$ start at every point on $\mathbb{R}$, and two particles "coalesce" into one upon collision. However, now the dynamics of particles after coalescence admit different interpretations. We propose three types of coalescence rules, namely

(1) Coin flip: When two particles collide, one is chosen with equal probability to "absorb" the other particle and continue its motion.

(2) Regenerate: When two particles collide, they both vanish and a new independent fBM particle is spawned at the point of collision.

(3) Pólya urn: Let $\alpha \geqslant 0$ be a fixed *Pólya index* (reminiscent of Pólya urn). Every particle starts with weight 1. When two particles of weights w_1 and w_2 collide, they respectively have probability $\frac{w_1^\alpha}{w_1^\alpha + w_2^\alpha}$ and $\frac{w_2^\alpha}{w_1^\alpha + w_2^\alpha}$ of winning. The winning particle absorbs the losing particle and continues its motion, with a new weight $w_1 + w_2$. Note that when $\alpha = \infty$ the particle with higher weight always wins, and when $\alpha = 0$ this is the coin-flip model.

For cBM, all the above coalescing rules are equivalent due to the strong Markov property. In contrast, fBM with Hurst index $H \neq 1/2$ is non-Markovian [16, Theorem 2.3], so one may expect that different coalescing rules would lead to different kinds of dependence on the past, and hence different versions of cfBM. This intuition is supported numerically; see Sec. II D

Although a rigorous construction of cfBM is currently not available, we study numerical simulations of cfBM with finitely many initial starting points that are sufficiently dense and equally spaced. The details of the simulation can be found in Sec. II C. We are particularly interested in cfBM with $H = 2/3$, where the point fields will have the same density scaling as KPZ models.

We will compare the point fields generated by the cfBM and by the *exponential corner growth model*. This is a last-passage percolation model known to belong in the KPZ universality class [7]. In this model, weights of independent and identically distributed exponential random variables are placed on each $(\mathbb{Z}_+)^2$-lattice point, and a boundary condition is specified on the non-negative x and y axes. The geodesics are the upright paths maximizing the sum of weights they visit. For details of this exactly solvable model, see [15]. The geodesics of this model can be generated efficiently. For the rest of this paper, by "LPP" we refer specifically to this exactly solvable model.

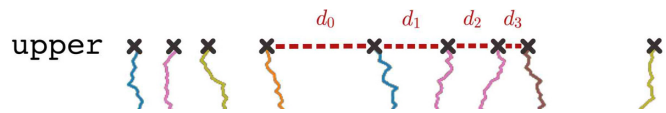

FIG. 2. d_k are identically distributed. $r_k = d_k/d_0$ is the *jump-k ratio*.

B. Test statistics

We are interested in the following questions:

(1) KPZ-like properties: Which model of cfBM has upper and/or lower point fields with similar statistics as that of LPP (KPZ)?

(2) Symmetry: The duality of cBM says that there is a joint realization of two cBMs: one forward in time and the other backward, with noncrossing paths. It follows that the upper and lower point fields of cBM are identically distributed. The symmetry of upper and lower point fields is also known to hold for LPP [17]. What about cfBM?

(3) Different coalescing rules: Does numerical evidence corroborate the expectation that different coalescing rules of the cfBM would lead to a difference in point field statistics?

This involves comparing the upper and lower point fields of different coalescing processes. With the translational invariance, these point fields are characterized by the distributions of distances between consecutive points and all finite joint distributions of such distances. In this paper we will use the p value from the *Kolmogorov-Smirnov* (K-S) test to compare the distributions of the following one-dimensional statistics:

Normalized consecutive point distance: We study the distribution of the distance between consecutive points in the point field, normalized by the sample mean. We denote this by δ_0.

Jump-k ratio: For fixed $k \geqslant 1$, we consider two intervals, k intervals apart, and call the ratio between their length the *jump-k ratio*, denoted by r_k (Fig. 2).

The random variables δ_0 and r_k, $k \geqslant 1$, can be defined for both the upper and the lower point fields.

C. Simulation

We simulated cfBM with the coalescing rule of coin-flip, regenerate and Pólya urn with a few values of α. We generate discretized steps of cfBm using the Python library *fbm* [18], with specifically the Davis-Harte algorithm [19]. The lengths of the discrete simulations are measured in the number of discrete steps, denoted by n. For our experiments, cfBMs are generated up to $n = 1024$ steps and LPP is generated up to $n = 4096$.

The starting positions occupy integer points $\{-k, -k + 1, \ldots, k - 1, k\}$, where we choose $k = 20 \times \text{round}(n^{2/3})$. The typical deviation of a sample path grows like $n^{2/3}$, hence the number of surviving points decay like $n^{-2/3}$. Thus, by the nth step, the empirical upper and lower fields contain

TABLE I. p values comparing *upper* fields of LPP and cfBM models.

	CF	$\alpha = 0.5$	$\alpha = 1$	$\alpha = 2$	$\alpha = 10$	$\alpha = \infty$	RG
δ_0	0.50	0.57	0.23	0.27	0.15	0.15	0.77
r_1	0.86	0.82	0.45	0.99	0.72	0.59	0.45
r_2	0.17	0.24	0.15	0.70	0.21	0.60	0.99
r_3	0.41	0.45	0.33	0.49	0.74	0.79	0.97
r_4	0.43	0.25	0.44	0.30	0.87	0.16	0.90
r_5	0.64	0.71	0.46	0.77	0.38	0.50	0.61
r_6	0.41	0.46	0.32	0.42	0.34	0.71	0.78

TABLE III. p values between upper and lower fields.

	CF	$\alpha = 0.5$	$\alpha = 1$	$\alpha = 2$	$\alpha = 10$	$\alpha = \infty$	RG	LPP
δ_0	0.75	0.15	0.16	<0.01	<0.01	<0.01	0.02	0.92
r_1	0.51	0.17	0.67	<0.01	<0.01	<0.01	0.22	0.66
r_2	0.25	0.58	0.87	<0.01	0.01	<0.01	0.12	0.73
r_3	0.55	0.17	0.51	0.01	<0.01	<0.01	0.52	0.99
r_4	0.96	0.35	0.44	<0.01	<0.01	<0.01	0.03	0.95
r_5	0.99	0.20	0.65	0.02	0.02	0.03	0.21	0.98
r_6	0.63	0.80	0.42	0.02	<0.01	0.01	0.11	0.42

approximately 40 points. Because both cfBM and LPP paths are homogeneous, it suffices to re-scale the point fields in the end.

Our statistical tests are based on a sample size of 500 independent cfBM/LPP, which gives rise to approximately $500 \times 40 = 20\,000$ samples for the consecutive point distance and jump-k ratios.

Before we perform the K-S test, two points from each end of the point fields are removed to account for finite-size effects. For instance, one end point—either the maximum or minimum (depending on the definition)—of the lower point fields is constant across samples, and is always equal to the maximum (resp. minimum) of the set of starting positions. Removing two points from each end of the point fields takes care of this problem.

Our documented code generating discrete cfBm and LPP and performing statistical tests, and the corresponding data banks, can be accessed on our GitHub repository [20].

D. Results

In this section, CF stands for the coin-flip model, RG stands for the regenerate model, and "$\alpha = x$" stands for the Pólya-urn model with index x.

In Table I we compare the upper point fields from cfBM models to that from LPP. Across the table we obtained high p values: the minimum is 0.15, while most p values are above 0.40. To compare, the last row of Table III contains p values computed from two identical distributions. Since the K-S test is based on the L^∞ distance between empirical CDFs and is sensitive to discretization and small differences, this provides numerical evidence of a strong similarity between the statistical properties of the upper point fields in the KPZ problem and in processes of coalescing fractional Brownian motions with the Hurst index 2/3.

We also compare the p values for the lower point fields in Table II. It can be seen that the p values are high for the coin-flip model. For the regenerate model the p values are low (<0.05) except for r_3. For the Pólya-urn models, the p values decrease as α increases, and almost vanish for $\alpha \geqslant 2$. This agrees with what we will see immediately below, that the coin-flip cfBM and LPP are the only two models that have symmetry between the upper and lower point fields. We note that the Pólya-urn model with $\alpha = 0$ is exactly the coin-flip model.

In Table III, we compare the statistics between the upper and lower point fields of each version of cfBM and the LPP model. The upper and lower point fields of the LPP model are known to be identically distributed, and the p values are in the range from 0.42 to 0.92. Using this range as a reference, Table III suggests that the coin-flip model is the only other model that can also possibly exhibit such symmetry.

There are intuitive reasons why the Pólya-urn model ($\alpha > 0$) and the regenerate model do not have such symmetry in the reverse time direction. In the Pólya-urn model, the weights of particles are monotonically increasing, and, in the regenerate model, the history of particles is erased upon collision. Lastly, we compare the point fields from cfBM with different coalescing rules in Table IV. We obtain extremely low p values from the lower point fields. This is expected and confirms that different coalescing rules yield different versions of cfBM. For the upper point fields, the p values are higher (>0.12), which agrees with the data in Table I. If one compares other statistics like the jump-k ratios, similar conclusions can also be drawn.

TABLE II. p values comparing *lower* fields of LPP and cfBM models.

	CF	$\alpha = 0.5$	$\alpha = 1$	$\alpha = 2$	$\alpha = 10$	$\alpha = \infty$	RG
δ_0	0.10	0.05	0.01	<0.01	<0.01	<0.01	<0.01
r_1	0.91	0.18	0.09	<0.01	<0.01	<0.01	<0.01
r_2	0.24	0.21	0.04	<0.01	<0.01	<0.01	0.01
r_3	0.19	0.04	0.01	<0.01	<0.01	<0.01	0.28
r_4	0.45	0.32	0.26	<0.01	<0.01	<0.01	0.02
r_5	0.50	0.09	0.08	<0.01	<0.01	<0.01	0.03
r_6	0.42	0.34	0.25	<0.01	<0.01	<0.01	0.04

TABLE IV. p values of δ_0, and upper (lower) triangle part corresponding to upper (lower) field.

	CF	$\alpha = 0.5$	$\alpha = 1$	$\alpha = 2$	$\alpha = 10$	$\alpha = \infty$	RG
CF		0.60	0.45	0.74	0.72	0.33	0.33
0.5	0.39		0.89	0.83	0.75	0.65	0.40
1	0.17	0.35		0.72	0.79	0.84	0.13
2	<0.01	0.03	0.15		0.99	0.99	0.22
10	<0.01	0.02	0.03	0.49		0.98	0.20
∞	<0.01	0.03	0.04	0.66	0.28		0.12
RG	<0.01	<0.01	<0.01	<0.01	<0.01	<0.01	

III. CONCLUSION

While most of the research in the field of KPZ was concentrated on the statistics of interface, or so-called height function, in this paper we suggest a more geometrical point of view. For many problems in the KPZ universality class one can naturally define the large scale point fields which can be viewed as places of concentration of polymers, or particles, and points of separation which can be viewed as shocks. The asymptotic statistical properties of these point fields are supposed to be universal, and in some sense encode the statistical properties of the interface.

In this paper we present an alternative model: coalescing fractional Brownian motions. This model normally would not be considered for belonging to the KPZ universality class. First of all, there is no height function which can be naturally associated with the process of coalescing Brownian motions (either fractional or standard). In other words, the interface interpretation is not available for our model. Second, the model is not related to any external disorder setting. Nevertheless, in this paper we present theoretical arguments and numerical evidence suggesting that the point fields arising from the model of cfBM have the same statistical properties as the points fields in the models of the KPZ class. Besides providing an approach to the problem of KPZ universality, our results suggest that the KPZ universality class is, in fact, much larger than was previously thought.

It was suggested in [12] that the statistical properties of the point fields are completely determined by the monotonicity properties, decorrelation conditions, and the requirement of a fixed asymptotic power law decay of the density of points fields. The arguments in favor of the above conjecture were based on the renormalization approach. The main idea was that, in the large-time limit, the probability law of a point field converges to a renormalization fixed point which is stable apart from one neutral direction corresponding to different values of the exponent of the power decay of the density. In the present paper we provide strong numerical support for such a universality of the point fields.

We stress again that cfBM can be considered for different Hurst indices. The case of the Hurst index $1/2$ corresponds to standard (nonfractional) Brownian motions. Universality in this case was studied in [21–23]. It was shown in [23] that the renormalization procedure can be viewed as the dynamical process of iteration by random monotone piecewise constant maps. The Hurst index $1/2$ corresponds to the situation when maps are identically distributed and independent. It was rigorously proved that in this case the fixed point is stable. Other Hurst indices correspond to the situation when different random monotone maps are correlated in time. The rigorous mathematical analysis in this case is a challenging problem.

ACKNOWLEDGMENT

K.K. acknowledges the support of the NSERC Discovery Grant No. RGPIN-2018-04510.

[1] M. Kardar, G. Parisi, and Y.-C. Zhang, Dynamic Scaling of Growing Interfaces, Phys. Rev. Lett. **56**, 889 (1986).

[2] D. Forster, D. R. Nelson, and M. J. Stephen, Large-distance and long-time properties of a randomly stirred fluid, Phys. Rev. A **16**, 732 (1977).

[3] J. Baik, P. Deift, and K. Johansson, On the distribution of the length of the longest increasing subsequence of random permutations, J. Am. Math Soc. **12**, 1119 (1999).

[4] K. Johansson, Shape fluctuations and random matrices, Commun. Math. Phys. **209**, 437 (2000).

[5] M. Prähofer and H. Spohn, Scale invariance of the PNG droplet and the Airy process, J. Stat. Phys. **108**, 1071 (2002).

[6] E. Cator and P. Groeneboom, Second class particles and cube root asymptotics for Hammersleys process, Ann. Probab. **34**, 1273 (2006).

[7] M. Balázs, E. Cator, and T. Seppäläinen, Cube root fluctuations for the corner growth model associated to the exclusion process, Electron. J. Probab. **11**, 1094 (2006).

[8] M. Balázs, J. Komjáthy, and T. Seppäläinen, Microscopic concavity and fluctuation bounds in a class of deposition processes, Ann. Inst. Henri Poincaré Probab. Statist. **48**, 151 (2012).

[9] G. Amir, I. Corwin, and J. Quastel, Probability distribution of the free energy of the continuum directed random polymer in 1 + 1 dimensions, Commun. Pure Appl. Math. **64**, 466 (2011).

[10] K. Matetski, J. Quastel, and D. Remenik, The KPZ fixed point, Acta Mathematica. **227**, 115 (2021).

[11] D. Dauvergne, J. Ortmann, and B. Virág, The directed landscape, arXiv:1812.00309.

[12] Y. Bakhtin and K. Khanin, On global solutions of the random Hamilton–Jacobi equations and the KPZ problem, Nonlinearity **31**, R93 (2018).

[13] R. A. Arratia, Coalescing Brownian motions on the line, Ph.D. thesis, University of Wisconsin– Madison, 1979 (unpublished), p. 134.

[14] M. Charles and C. M. Newman, A surface view of first-passage percolation, in *Proceedings of the International Congress of Mathematicians, August 3–11, 1994, Zürich, Switzerland* (Birkhäuser, Basel, 1995), pp. 1017–1023.

[15] T. Seppäläinen, Existence, uniqueness and coalescence of directed planar geodesics: Proof via the increment-stationary growth process, Ann. Inst. H. Poincaré Probab. Statist. **56**, 1775 (2020).

[16] I. Nourdin, *Selected Aspects of Fractional Brownian Motion*, Bocconi & Springer Series No. 4 (Springer, Milan, 2012).

[17] L. P. R. Pimentel, Duality between coalescence times and exit points in last-passage percolation models, Ann. Probab. **44**, 3187 (2016).

[18] C. Flynn, Fractional Brownian motion realizations, in The Python Package Index, https://pypi.org/project/fbm/.

[19] R. B. Davis and D. Harte, Tests for Hurst effect, Biometrika **74**, 95 (1987).

[20] Codes and data available at https://github.com/neo-yin-math/cfBm-KPZ.

[21] V. V. Piterbarg, *Expansions and Contractions of Stochastic Flows* (University of Southern California, Los Angeles, 1997).

[22] L. I. Piterbarg and V. V. Piterbarg, Intermittency of the tracer gradient, Commun. Math. Phys. **202**, 237 (1999).

[23] K. Khanin and L. Li, On asymptotic behavior of iterates of piecewise constant monotone maps, arxiv:2110.09731.